MRS Advances © 2018 Materials Research Society
DOI: 10.1557/adv.2018.299

p-n Based Photoelectrochemical Device for Water Splitting Application Alpha-Hematite (α-Fe_2O_3)-Titanium Dioxide (tio_2) as N-Electrode & Polyhexylthiophene (rrphth) - Nanodiamond (ND) as P-Electrode

Hussein Alrobei[1,2], Hye Young Lee[3], Ashok Kumar[1], and Manoj K. Ram[4,5]

[1]*Department of Mechanical Engineering, University of South Florida, Tampa, Florida 33620, USA*

[2]*Department of Mechanical Engineering, Sattam bin Abdulaziz University, Alkharj, Saudi Arabia*

[3]*Department of Materials Science and Engineering, University of South Florida, Tampa, Florida 33620, USA*

[4]*Clean Energy Research Center, University of South Florida, Tampa, FL 33620, USA*

[5]*PolyMaterials APP, LLC, 3802 Spectrum Blvd, Suite 145, Tampa, FL -33612, USA*

ABSTRACT

Recently, photoelectrochemical (PEC) water splitting using semiconductor photoanode has received great attention due production of hydrogen through clean energy. The alpha hematite (α Fe_2O_3) is one of the candidate amongst photoanodic materials, which is chemically stable, abundant in nature with a band gap of 2.0-2. 2eV allowing to be harvesting in the visible light. However, it has also drawn back due to high recombination rate of electron–hole pair revealing the low concentration of charges and lower device performance. In common with α-Fe_2O_3, the titanium dioxide (TiO_2) has been known as one of the most explored photoanode electrode material due to its physical and chemical stability in aqueous and non-toxicity. However, TiO_2 has large bandgap (3.0-3.2 eV) that results in absorbing UV light and very small part of visible region. Incorporation of TiO_2 in α-Fe_2O_3 could achieve better efficiencies as photoanode materials by enhancing the electric conductivity, limited hole diffusion length, and both materials can absorb light in both UV and visible spectrum range. However, the photoanodic properties of α-Fe_2O_3 with different concentrations of TiO_2 are mostly unknown. Under this work, α-Fe_2O_3-TiO_2 nanomaterial was synthesized using a hydrothermal method. The α-Fe_2O_3-TiO_2 nanomaterials containing different weight percentage (2.5, 5, 16, 25, and 50) of TiO_2 to α-Fe_2O_3 were characterized using SEM, XRD, UV-Vis, FTIR and Raman techniques, respectively. The electrochemical properties of α-

Fe_2O_3-TiO_2 nanomaterials were investigated by cyclic voltammetry and chronoamperometry techniques, respectively.

INTRODUCTION

The great attention has been paid for the production of hydrogen as an alternative energy by the photoelectrochemical (PEC) splitting water processes [1, 2]. The transition metal oxide semiconductors have been used as photocatalyst for water PEC based splitting applications [3-6]. Among materials, α-Fe_2O_3 is one of the extensively explored material, and has advantages for production of hydrogen in PEC process: chemically suitable for electrolytes (PH > 3), relatively narrow bandgap (2.0 - 2.2eV), abundant and inexpensive [7, 8]. Due to the short electron-hole pair time (<10 ps) and hole diffusion length (2-4 mm) which cause high recombination rate of photo-generated carriers in the bulk, hematite based water splitting has lower efficiency than that of the theoretical (12.6 mA/cm^2), and have restricted PEC applications [9, 10]. On the surface of hematite based water splitting, in addition, the oxidation-reduction seems to delay due to the kinetics of the interfacial extraction of hole, and then might be accompanied by increased charge recombination and the decline of efficiency [9, 11]. To improve photoelectrochemical properties, TiO_2 has been investigated because of low cost for the fabrication of photoelectrochemical stability and inexpensive[12, 13]. However, TiO_2 has also significant limitations. Firstly, excitation is generated in response to UV regions. Secondly, the PEC device, which has been fabricated with TiO_2 often, has short diffusion length of excitation [14, 15]. To solve above limitations, there are some suggestions of reducing bandgap that allows PEC device to absorb visible region and making large contact area with electrolyte that allows PEC device to split of electron-hole pairs [14, 16]. As gathering advantages of both metal oxide materials, TiO_2 with Fe_2O_3 film was shown as increasing contacting area with electrolyte reducing e-h recombination and shift light absorption along with visible region [9, 17, 18].

However, the property change of hematite photoanode by TiO_2 different concentrations is unknown exactly. Under this work, nanocomposite α-Fe_2O_3-TiO_2 nanomaterials with different concentrations (50%, 25%, 16%, 5% and 2.5% of TiO_2) were synthesized by hydrothermal method, and were dried at 300 °C and 500°C, respectively. The physical properties of α-Fe_2O_3-TiO_2 nanomaterials were compared by using SEM, XRD, UV-Vis, FTIR and Raman measurements. The photoelectrochemical properties were also estimated by chronoamperometry technique.

EXPERIMENT DETAILS AND CHARACTERIZATION

Iron chloride ($FeCl_3$), titanium (IV)-isopropoxide solution (TTIP), and sodium hydroxide (NaOH) were used to synthesize the α-Fe_2O_3-TiO_2 nanomaterials. Potassium bromide (KBr, Aldrich) which was purchased from Sigma-Aldrich co., was used for making FTIR sample pellets. Acrylic acid (Aldrich) was used by mixing the synthesized material for fabricating film. To measure electrochemical properties, indium tin oxide (ITO) glasses coated was used to coat α-Fe_2O_3-TiO_2 which worked as working electrode. We have used, silicon wafers coated with polyhexylthiophene (RRPHTh)-nanodiamond (ND) as counter electrode.

α-Fe_2O_3-TiO_2 nanomaterials were synthesized by hydrothermal process. Equation 1 shows the chemical reaction equation. The synthesized α-Fe_2O_3-TiO_2 nanomaterials were obtained by changing different concentrations of reactant materials, which were $FeCl_3$ and TTIP. To obtain different concentrations of TiO_2 (50%, 25%,

16%, 5% and 2.5%), the amount of $FeCl_3$ and TTIP were put into the round bottom flask with DI water (450 ml), respectively. To dissolve the above materials, the resulting solution was stirred with magnetic stir bar, and the flask was put on the hotplate at 60 °C for an hour. After an hour, NaOH solution (50mL) was added to the resulting solution and connected up to reflux condenser. Reaction temperature was maintained at 90 °C for chemical reaction, and reaction time was maintained for 24 hours. The solution was separated as the α-Fe_2O_3-TiO_2 nanomaterial and residues by using filter paper. The α-Fe_2O_3-TiO_2 nanomaterial was washed using DI water twice in order to remove the impurities. Then, α-Fe_2O_3-TiO_2 nanomaterial was cooled at room temperature for 12 hours. The α-Fe_2O_3-TiO_2 nanomaterial was dried at 300 °C, and 500 °C for 2 hours for each and dried α-Fe_2O_3-TiO_2 nanomaterial and further grinded by using ball-milling machine. TiO_2 nanomaterials was fabricated with 0.05M of TTIP, and subsequently dried at 500 °C for 3 hours using similar condition of α-Fe_2O_3-TiO_2 nanomaterial synthesis process.

$$4FeCl_3 + Ti\{OCH(CH_3)_2\}_4 + 5NaOH \xrightarrow[at\ 90°C\ for\ 24\ hours\ \&\ drying]{} 2(2TiO_2 - Fe_2O_3) + \alpha \quad (eq1)$$

The α-Fe_2O_3-TiO_2 nanomaterial and KBr powder were mixed and applied hydraulic press for obtaining the pellets. The Fe_2O_3 pellet and TiO_2 pellet were prepared for comparative analysis. To fabricate film-type specimens, the α-Fe_2O_3-TiO_2 nanomaterial was mixed with little acetic acid for obtaining the colloidal materials. The colloidal α-Fe_2O_3-TiO_2 materials were used to coat on ITO glasses (2cm ×2.5 cm) and were cured at 100 °C for an hour. The counter electrode was fabricated by immersing pieces of Si-wafer in RRPHTh- ND colloidal solution [19].

The X-ray diffraction (XRD), SEM and Raman spectroscopy were performed by using powder form samples. For electrochemical properties, a Potentiostat/Galvanostat instrument (Radiometer Analytical, Volta lab 40 PGZ301) was utilize. To measure cyclic voltammetry and chronoamperometry properties, the working electrode (α-Fe_2O_3-TiO_2 /ITO) and the counter electrode (RRPHTh-ND /Si) were immersed in NaOH (0.1M) solution as electrolyte and connected to the equipment using clips.

UV-Vis SPECTROSCOPY

The UV-Vis characterizations on α-Fe_2O_3-TiO_2 nanomaterials film on glass substrates was measured using UV-visible spectrophotometer (Jasco- V-670 absorption spectrometer). Figure 1 and Figure 2 UV-Vis spectra of TiO_2, α-Fe_2O_3 and α-Fe_2O_3-TiO_2 that were prepared at various concentrations of TiO_2 to α-Fe_2O_3, and dried at 300 °C and 500°C, respectively. The absorption spectra were able to obtain from the UV-Vis spectroscopy by measuring the sample holder that contained powder formed sample dissolved in DI water. Table 1 and 2 listed the absorption peaks of all samples. For comparison, the α-Fe_2O_3 nanomaterial exhibits absorption in the vicinity of 300 nm in the UV region and broad weak absorption at 400-600 nm in the visible region (figure 1&2a). For the TiO_2 nanomaterials, two absorption bands in the UV regions at 237 nm and 327nm are observed. In addition, there are also few very weak absorption bands at 428 nm and 488nm in visible region (figure 1&2). Figure 1 (b-f) b- shows the UV-Vis absorption bands for five different concentrations TiO_2 (2.5%, 5%, 16%, 25% and 50%) to α-Fe_2O_3 nanomaterials that were dried at 300 °C. Figure 2(b-f) shows absorption band for α-Fe_2O_3-TiO_2 nanomaterials dried at 500 °C with same condition. From the figure 1

and figure 2, drying temperature seems to have insignificant influence on absorption bands of the material. For high concentration of TiO_2 (16, 25, and 50%) samples, the absorption bands are similar to that of TiO_2 sample. Thus, absorption bands exhibit the characteristic of TiO_2 nanomaterial. For the low concentration TiO_2 (5 and 2.5 %) samples, the absorption bands appear for the α-Fe_2O_3-TiO_2 nanomaterials which are different spectra than Fe_2O_3 and TiO_2 samples. The absorption bands at 238, 270 and 320 nm begin to exhibit in UV region. In addition, strong absorptions appear near 428 and 540 nm in visible region. Thus, α-Fe_2O_3-TiO_2 nanomaterial with small quantity of TiO_2 seems to be red shifted due to the TiO_2 nanomaterials showing the improvement in absorption in the range of 400-600nm[20, 21].

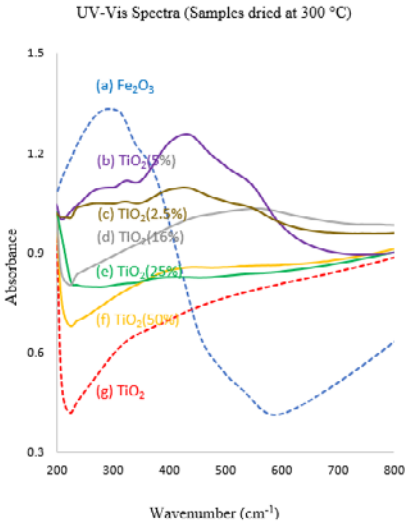

Figure 1 UV-Vis absorption spectra of α Fe_2O_3-TiO_2 dried at 300 °C

Table 1: The peaks of each α-Fe_2O_3-TiO_2 dried at 300 °C

	Wavenumber (cm^{-1})
TiO_2	237, 327, 428, 488
TiO_2 (50%)	236, 397, 438, 524, 607
TiO_2 (25%)	238, 321, 386, 532
TiO_2 (16%)	236, 453, 561
TiO_2 (5%)	279, 325, 428, 534
TiO_2 (2.5%)	216, 236, 264, 329, 432, 537
Fe_2O_3	299, 364, 488, 537

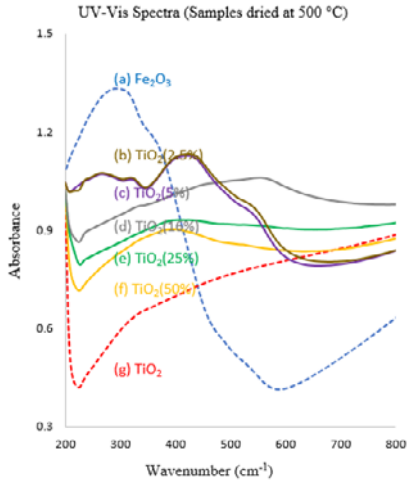

Figure 2 UV-Vis absorption spectra of α-Fe_2O_3-TiO_2 dried at 500 °C

Table 2: The peaks of each α-Fe_2O_3-TiO_2 dried at 300 °C

	Wavenumber (cm^{-1})
TiO_2	237, 327, 428, 488
TiO_2 (50%)	235, 334, 398, 526
TiO_2 (25%)	236, 404, 432, 528
TiO_2 (16%)	236, 335, 456, 560
TiO_2 (5%)	230, 271, 329, 428, 544
TiO_2 (2.5%)	218, 239, 268, 322, 428, 544
Fe_2O_3	299, 364, 488, 537

FTIR MEASUEMENT

The FTIR measurement on nanomaterials was made using KBr pellets in transmission mode using FTIR spectrophotometer (Perkin-Elmer spectrum one). The data was obtained after averaging the 16 scans for each sample recorded from 400 to 2000 cm^{-1}. Figure 3 shows the Fe_2O_3, TiO_2, and α-Fe_2O_3-TiO_2 nanomaterials with different concentrations of TiO_2 (50, 25, 16, 5 and 2.5%) at 500 °C of drying. The samples were measured by using transmission mode from 400 to 2000 cm^{-1}. The infrared bands of all samples are shown as Table 3. The weak band near 1630 cm^{-1} is relevant to H-O-H bending vibration mode, since moisture on the surface of sample is adsorbed [22]. The TiO_2 samples shows broad band in range of 400 to 700 cm^{-1} which is ascribed to the stretching vibration of Ti-O-Ti and Ti-O bridge bond [22, 23]. On the other hand, the Fe_2O_3 sample exhibits the broad band at 580 cm^{-1}, which is ascribed to the Fe-O(metal-oxygen) stretching-mode [24]. For the α-Fe_2O_3-TiO_2 nanomaterial, infrared bands at 460 and 560 cm^{-1} become stronger as the concentration of TiO_2 is lower. Both infrared bands at 460 and 560 cm^{-1} seem to be corresponding to the α-Fe_2O_3-TiO_2 nanomaterial lattice.

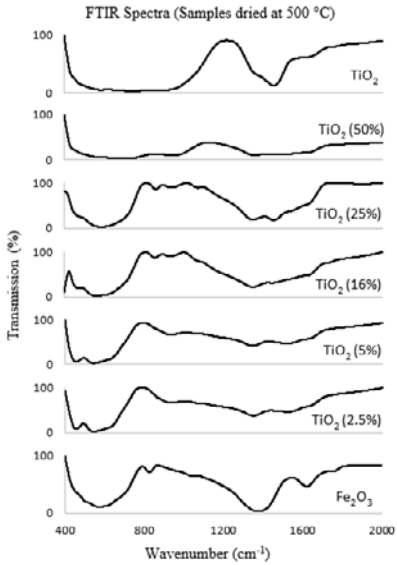

Figure 3 FTIR spectra of α-Fe_2O_3-TiO_2 dried at 500 °C

Table 3: The infrared bands of each α-Fe_2O_3-TiO_2

	Wavenumber(cm^{-1})
TiO_2	583, 651, 713, 767, 898, 1452, 1624, 1751
TiO_2 (50%)	442, 483, 588, 720, 950, 1354, 1451, 1541, 1620
TiO_2 (25%)	473, 582, 859, 942, 1070, 1346, 1452, 1542, 1617
TiO_2 (16%)	469, 554, 856, 932, 1066, 1346, 1449, 1622, 1726
TiO_2 (5%)	454, 540, 932, 1064, 1184, 1341, 1521, 1615
TiO_2 (2.5%)	456, 542, 928, 1064, 1170, 1346, 1527, 1629
Fe_2O_3	454, 501, 561, 582, 825, 1041, 1373, 1621, 1757

Raman Spectroscopy

Figure 4 shows the Raman spectra of the Fe_2O_3, TiO_2, and α-Fe_2O_3-TiO_2 nanomaterials with different concentrations of TiO_2 (50, 5, and 2.5%) with heat treatment at 500 °C. Table 4 indicated the Raman peak of all sample. The Fe_2O_3 sample exhibits peaks of 225, 295, 409 cm^{-1} that are assigned to hematite. Namely, the lines at 225 cm^{-1} is assigned to the A_{1g} vibration mode and 296 and 409 cm^{-1} are assigned to the E_g vibration mode [25, 26]. The TiO_2 samples shows 205, 275, 434, 633 and 823 cm^{-1}. The TiO_2 sample includes both anatase and rutile phases; Raman shifts nearby 205, and 633 cm^{-1} for anatase phase and nearby 434 and 823 cm^{-1} for rutile [27-29].

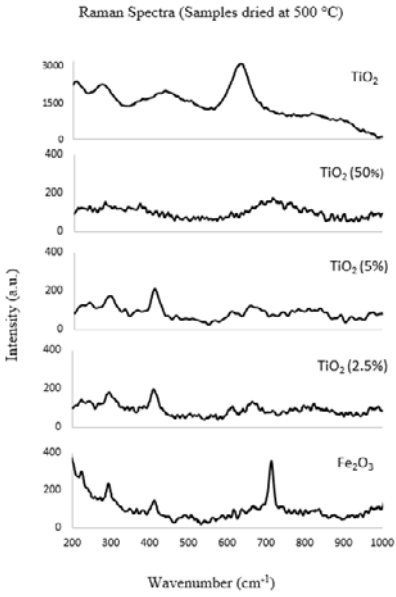

Figure 4 Raman spectra of α-Fe_2O_3-TiO_2 dried at 500 °C

Table 4: The peaks of each α-Fe_2O_3-TiO_2

	Wavenumber (cm^{-1})
TiO_2	205, 275, 434, 633, 823
TiO_2 (50%)	215, 278, 375, 717, 978
TiO_2 (5%)	232, 288, 406, 628, 664, 819, 975
TiO_2 (2.5%)	225, 243, 299, 406, 614, 664, 819, 967
Fe_2O_3	225, 295, 409, 712, 824, 970

Scanning Electron Microscopy (SEM)

THE SEM pictures of nanomaterials were measured using Field Emission Hitachi S800 Scanning Electron Microscope. Figure 5 shows scanning electron microscopy (SEM) images of Fe_2O_3, TiO_2 and α-Fe_2O_3-TiO_2 with different concentration of TiO_2 (50, 5 and 2.5 %) samples. Figure 5a-b show SEM images of synthesized TiO_2 and Fe_2O_3 nanomaterial samples respectively, and average diameter of particles are less than 10μm. On the other hand, figure 5c-e shows SEM images of α-Fe_2O_3-TiO_2 with different concentration of TiO_2 (50, 5 and 2.5 %) nanomaterials. Figure 5d-f show the urchin–like nanostructure consisting of nanowires on the particle, thus the average particle size is over 10 μm. The urchin-like nanostructure obtains more surface area, which may improve the effective interface of α-Fe_2O_3 and improve performance of water splitting application [18, 26, 30].

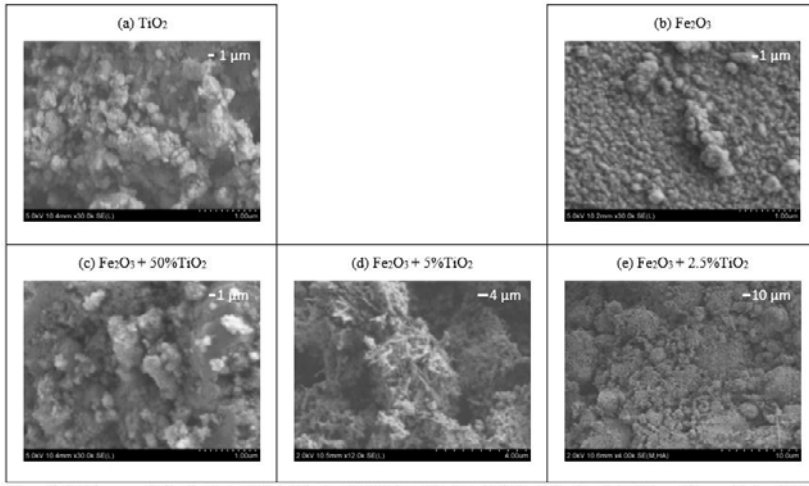

Figure 5 SEM images of (a) α-Fe_2O_3 (b) TiO_2 (c) Fe_2O_3 + 50%TiO_2 (d) Fe_2O_3 + 5%TiO_2 (e) Fe_2O_3 + 2.5%TiO_2 which are dried at 500 °C

CHRONOAMPEROMETRY

The electrochemical studies on various α-Fe_2O_3-TiO_2 nanomaterial films were conducted using Potentiostat/galvanostate of model "PGZ 301 Dynamic EIS voltammetry" from Volta lab. The chronoamperometry curve was measured by using two electrodes consisting of α-Fe_2O_3-TiO_2 nanomaterial (50% of TiO_2 dried at 500 °C) film as working electrode and RRPHTh-ND as counter electrode. 1M of NaOH solution was utilized as electrolyte. The electrochemical photo response was measured by switching on/off the lamp (60W). Figure 6 shows the chronoamperometry photocurrent curve with time (sec) for oxidation-reduction reaction of α-Fe_2O_3-TiO_2 film. When charge potential was at 1000 mV, current density was at 120µm/cm^2 of maximum and 90µm/cm^{-2} of average (Figure 6a), when charge potential was at 2000 mV, current density was at 800µm/cm^{-2} of maximum and 300µm/cm^{-2} of average (Figure 6b). The increase of potential shows the larger current density due to oxidation of water.

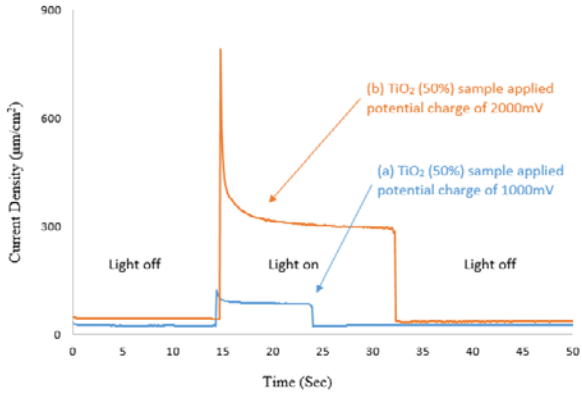

Figure 6. The photocurrent responses for α-Fe_2O_3-TiO_2 nanomaterial sample with 50% of TiO_2 heat treatment at 500 °C. (a) working electrode applied with 1000mV of charge potential, (b) is applied with 2000 mV of charge potential

CONCLUSIONS

The α-Fe_2O_3. TiO_2 nanomaterial was synthesized with different percentages of TiO_2. The α-Fe_2O_3-TiO_2 nanomaterial is able to absorb visible region. The low concentration of TiO_2 (5% and 2.5%) nanomaterial may be concerned of changing the structure of α-Fe_2O_3 nanomaterials based on SEM images. The urchin- nanostructure improves the effective interface of α-Fe_2O_3 and also enhances the performance of water splitting application. The TiO_2 sample in α-Fe_2O_3-TiO_2 nanomaterial shows the presence of both phases such as anatase and rutile. In addition, production of photocurrent seems to be improving with illuminating the electrode based on α-Fe_2O_3-TiO_2 nanomaterial. TiO_2 nanomaterial contributes to improve the performance of PEC device based on α-Fe_2O_3-TiO_2 nanomaterial electrode by shifting absorbing region of light, and by expanding the contact area with electrolyte on α-Fe_2O_3-TiO_2 surface. The increase of potential shows the larger current density due to oxidation of water using a α-Fe_2O_3-TiO_2 nanomaterial film.

REFERENCES

1. B.-R. Kim, H.-J. Oh, K.-S. Yun, S.-C. Jung, W. Kang and S.-J. Kim, *Progress in Organic Coatings* **76**, 1869 (2013).
2. J.D. Ruth, L.M. Hayes, D.R. Martin and K. Hatipoglu, An overview of photoelectrochemical cells (PEC): Mimicking nature to produce hydrogen for fuel cells, in SoutheastCon, 2017 (IEEE2017), pp. 1.
3. M. Ni, M.K. Leung, D.Y. Leung and K. Sumathy, *Renewable and Sustainable Energy Reviews* **11**, 401 (2007).
4. T. Hisatomi, J. Kubota and K. Domen, *Chemical Society Reviews* **43**, 7520 (2014).
5. A. Kudo, *Catalysis Surveys from Asia* **7**, 31 (2003).
6. J. Deng, J. Zhong, A. Pu, D. Zhang, M. Li, X. Sun and S.-T. Lee, *Journal of Applied Physics* **112**, 084312 (2012).
7. A. Murphy, P. Barnes, L. Randeniya, I. Plumb, I. Grey, M. Horne and J. Glasscock, *International journal of hydrogen energy* **31**, 1999 (2006).
8. A. Watanabe and H. Kozuka, *The Journal of Physical Chemistry B* **107**, 12713 (2003).
9. X. Li, P.S. Bassi, P.P. Boix, Y. Fang and L.H. Wong, *ACS applied materials & interfaces* **7**, 16960 (2015).
10. K. Sivula, F. Le Formal and M. Grätzel, *ChemSusChem* **4**, 432 (2011).

11. S.J. Moniz, S.A. Shevlin, D.J. Martin, Z.-X. Guo and J. Tang, *Energy & Environmental Science* **8**, 731 (2015).
12. Y.J. Hwang, C. Hahn, B. Liu and P. Yang, *Acs Nano* **6**, 5060 (2012).
13. A. Fujishima, T.N. Rao and D.A. Tryk, *Journal of Photochemistry and Photobiology C: Photochemistry Reviews* **1**, 1 (2000).
14. S. Choudhary, S. Upadhyay, P. Kumar, N. Singh, V.R. Satsangi, R. Shrivastav and S. Dass, *International journal of hydrogen energy* **37**, 18713 (2012).
15. M. Zhou, X.W.D. Lou and Y. Xie, *Nano Today* **8**, 598 (2013).
16. X. Chen, C. Li, M. Grätzel, R. Kostecki and S.S. Mao, *Chemical Society Reviews* **41**, 7909 (2012).
17. A. Malik, S. Hameed, M. Siddiqui, M. Haque and M. Muneer, *International Journal of Photoenergy* **2013** (2013).
18. J. Zhu, J. Ren, Y. Huo, Z. Bian and H. Li, *The Journal of Physical Chemistry C* **111**, 18965 (2007).
19. M.K. Ram, H. Gomez, F. Alvi, E. Stefanakos, Y. Goswami and A. Kumar, *The Journal of Physical Chemistry C* **115**, 21987 (2011).
20. O. Zandi, B.M. Klahr and T.W. Hamann, *Energy & Environmental Science* **6**, 634 (2013).
21. X. Yang, R. Liu, C. Du, P. Dai, Z. Zheng and D. Wang, *ACS applied materials & interfaces* **6**, 12005 (2014).
22. C. Johnston, G. Sposito and C. Erickson, *Clays and Clay Minerals* **40**, 722 (1992).
23. D. Zhang, *High Energy Chemistry* **47**, 177 (2013).
24. M. Ahmadi Golsefidi, F. Abbasi, M. Abrodi and Z. Abbasi, *Journal of Nanostructures* **6**, 64 (2016).
25. J.I. Peña-Flores, A.F. Palomec-Garfias, C. Márquez-Beltrán, E. Sánchez-Mora, E. Gómez-Barojas and F. Pérez-Rodríguez, *Nanoscale research letters* **9**, 499 (2014).
26. D. De Faria, S. Venâncio Silva and M. De Oliveira, *Journal of Raman spectroscopy* **28**, 873 (1997).
27. P.C. Ricci, C.M. Carbonaro, L. Stagi, M. Salis, A. Casu, S. Enzo and F. Delogu, *The Journal of Physical Chemistry C* **117**, 7850 (2013).
28. T. Ohsaka, F. Izumi and Y. Fujiki, *Journal of Raman spectroscopy* **7**, 321 (1978).
29. T. Mazza, E. Barborini, P. Piseri, P. Milani, D. Cattaneo, A.L. Bassi, C. Bottani and C. Ducati, *Physical Review B* **75**, 045416 (2007).
30. N. Mirbagheri, D. Wang, C. Peng, J. Wang, Q. Huang, C. Fan and E.E. Ferapontova, *Acs Catalysis* **4**, 2006 (2014).